Synthesis and Characterization of Multilayer Thin Films using Spray Pyrolysis Technique

A project report for partial fulfilment of requirements for degree of
Integrated Master of Science
in
Physics

Submitted by
Soumya Ranjan Sahu
410PH5049

Supervised by
Prof. Prakash Nath Vishwakarma
Department of Physics and Astronomy
National Institute of Technology Rourkela

Department of Physics and Astronomy
National Institute of Technology, Rourkela
Rourkela, Odisha, India, 769008

CERTIFICATE OF APPROVAL

This is to certify that the work done in the thesis entitled "**Synthesis and Characterization of Multilayer Thin Films**" by **Soumya Ranjan Sahu** towards partial fulfilment of the requirements for the award of Master of Science degree in PHYSICS by National Institute of Technology, Rourkela, is an authentic work carried out by him under my supervision and guidance. The work has not been submitted elsewhere before for any other academic degree or award.

Dr. Prakash Nath Viswakarma
Department of Physics and Astronomy
National Institute of Technology, Rourkela
India

Acknowledgement

In reaching the end of the long journey that has created this thesis, I sincerely wish to thank the ones who shared its path with me. Above all else I would like to thank my supervisor, Dr. Prakash Nath Vishwakarma, for his support for as far back as two years, giving precious understanding and useful feedback to the research I have done.

I might likewise want to thank the following individuals who have helped me greatly in this project work. Dr. D. Behera and Prof. Simanchala Panigrahi, to permit me to utilize some of their laboratory instruments. Miss Jasashree Ray, Mr. Achyuta Kumar Biswal and Mr. Sourav Kuila for the computerization of the assembly, their significant suggestions and the most required supporting hands amid experiments. Mr. Kailash Chandra Das for productive discussions.

I would like to extend my gratitude to my parents, for their blessings, encouragement and moral support.

Soumya Ranjan Sahu
410PH5049
National Institute of Technology Rourkela
India

Contents

List of Figures

Chapter 1

Introduction

Thin films have shaped our everyday life in many ways. They have given us compact, easy to use and light products to make our life easier. Integrated circuits, those are a necessary part of today's electronic gadgets, use thin film technology for their fabrication. Thin film layer thickness vary from a fraction of nanometer to several micrometers. Thin films are attractive not just because of their smaller dimension, but also for their interesting properties as some thin film properties are different from the bulk.

1.1 ZnO

ZnO is a semiconducting material. It has a direct bandgap of 3.37 eV at room temperature. It has high chemical stability and low dielectric constant. ZnO also shows a large exciton binding energy of 60MeV and large electrochemical coupling coefficient. [1] Low material cost, availability to large area substrate is helpful in industrial applications. ZnO also shows the amenability to wet chemical etching and a high radiation resistance. [2] Its high electron mobility is used in applications such as transparent electrodes in LCDs and also in heat protecting windows. ZnO has high thermal conductivity and UV protection properties.

1.1.1 Physical properties of ZnO

Table 1.1: Physical properties of ZnO

Molar Mass	81.409 gm/mol
Appearance	White solid
Band gap	3.37 eV(Direct Bandgap)
Refractive index	2.00

1.1.2 Crystal structure of ZnO

Crystalline Zinc oxide appears in two main forms. They are hexagonal wurtzite [3] and cubic zincblende. At ambient conditions, the first one is more stable. This is why wurtzite structure is most common. If the substrate is of cubic lattice structure, then the cubic zincblende structure can be stable at room temperature. ZnO shows piezoelectricity

and pyroelectricity properties. While hexagonal and zincblende ZnO shows the formaer, hexagonal ZnO shows the later. The lattice constants are a = 3.25 and c = 5.2 . the ratio c:a is approximately 1.60 which is close to the ideal value for hexagonal cell c:a = 1.633 [4] .The bonding in ZnO is largely ionic. This is consistent with the fact that most group II-Vi materials show large ionic bonding in oxides. The radii is of 0.074 nm for Zn2+ and 0.140 nm for O2 in case of ZnO. This large ionic bonding property is responsible for the stable wurtzite structure rather than zinc blende. The strong piezoelectricity of ZnO is also the result of large ionic bonding. Although there is a polar Zn-O bond and, Zinc and Oxygen planes are electrically charged, the surfaces show no reconstruction to nuetrilize the planes. This anomaly is yet to be understood. [5]

1.2 $BiFeO_3$

Bismuth ferrite (BFO) is a multiferroic material which shows antiferromagnetism with a $T_N \approx 643$ K [6] and ferroelectricity with a $T_C \approx 1143$ K. [7] Due to their technological potential, increasing effort is devoted to studying multiferoic thin films. These materials are expected to be the basis of a novel memory, transducers and MEMS devices by a combination of dielectric and magnetic ordering.

1.2.1 Multiferroic materials

Multiferroic materials are the materials those exhibits more than one primary ferroic order parameter in a single phase. Some multiferroics show coupling between these primary order parameters. The basic primary oeder parameters can be listed as ferromagnetism, ferroelasticity, ferroelectricity and ferrotoroidicity. These materials show a well defined hysteresis loop by providing electric, magnetic or mechanical energy. Rare earth magnetites or ferrites or transition metal perovskite oxides are multiferroic materials. $TbMnO_3$,$TbMn_2O_5$, $HoMn_2O_5$, $LuFe_2O_4$, $BiFeO_3$, $BiMnO_3$, $LiCu_2O_2$, $BaNiF_4$ and $ZnCr_2Se_4$ are some examples of this. Multiferroic materials have been recognised for their use in potential device applications. Multi-state memory elements, sensors which can be used in multi-modes, spintronic devices, transducer, FeRAM etc. have the tremendous application of multiferroic materials.
Recently, multiferroic materials have been classified as type-1 and type-2 multiferroics. In type-1 multiferroics, sources of ferroelectricity and ferromagnetism are different and independent. In type-2 multiferroics, these states have a strong couplung with each other.

1.2.2 Physical properties of $BiFeO_3$

Table 1.2: Physicak properties of $BiFeO_3$

Molar Mass	45.8088 gm/mol
Appearance	Brown
Band gap	2.67 eV
Tc	1143 K

1.2.3 Crystal structure of $BiFeO_3$

Perovskite-oxide has a structural formula of ABO_3 . In this case, A is a large cation such as Bi3+ , Ba2+ or Pb2+. B is a medium-sized cation such as Fe3+, Ti4+, or Zr4+. Oxygen anions form cages and these cations are located in those cages. There exist a subgroup of the perovskite family that shows ferroelectric property. Above the curie temperature, they are cubic. However, below the curie temperature, they become polar non cubic. Above the curie temperature, the cations are located at the center of an oxygen octahedron. Below the curie temperature, they shift to a off- center. This shift of the cations in oxygen can be controlled by applying an external electric field. The structure and properties of the singlecrystal form of BFO have been extensively studied. It has a rhombohedrally distorted perov skite structure [8] at room temperature. It has a lattice parameter of a = b = c = 0.3965 nm and $\alpha = 89.30$ at room temperature. [8, 9, 10]

1.3 Multi-layer thin films

Multilayer thin films are becoming increasingly important in the development of faster, smaller and more efficient electronic and optoelectronic devices. One of the motivations of applying multilayer structures is to modify the optical properties of materials.

Multi layer thin films has been recognized for their applications in many fields. In case of bilayers, the first layer appears as a substrate for the second layer. This changes the property of the whole system. When the first layer and the second layers are different, the whole system behaves like a new material. Multilayer thin films can be used in optical communication systems. [11]. Using multi layer thin films, we can change the magnetic property of materials. [12]. Recent research shows that we can use multilayer ferroelectric thin films for pyroelectric applications. [13].

1.4 Spray Pyrolysis technique

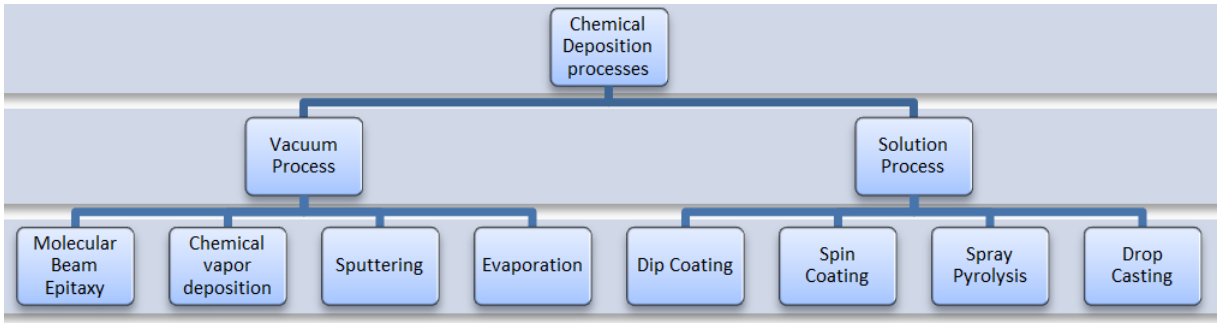

Figure 1.1: Various chemical deposition processes

Spray pyrolysis technique is one of the method to prepare thin films. It is cost effective and takes a short time span to synthesize thin films. Spray pyrolysis technique, as compared with other method shows capability of uniform deposition and large-area deposition. The fabrication of all kinds of industrial procedure is based upon the conditions of synthesis, resulting on the properties and performance of the obtained product.

There are various parameters in spray pyrolysis to enhance the quality of the thin film. Thes parameters include the concentration of the precursor solution, the spray rate, the temperature of the substrate and the angle of spray. With the help of spray pyrolysis technique, thin films can be synthesized in ambient pressure. Spray pyrolysis technique is specialy useful for low cost applications.

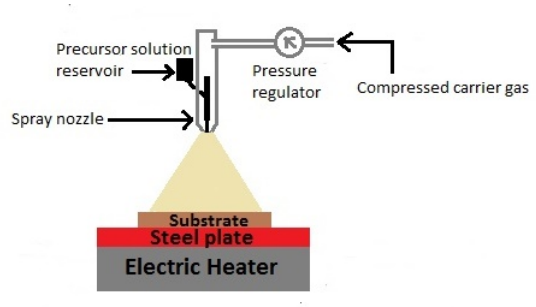

Figure 1.2: Schematic diagram of Spray Pyrolysis

The mechanism that follows in this is as follows. Precursor drops pass through three major steps. They are ,[14]

- Because of evaporation, there is a decrease in the drop size ocurs.
- The precursor converts into oxides
- formation of solid particles

The formation of solid particles goes through two mechanisms. They are conventional one-particle-per-drop mechanism, which is also called intraparticle reaction and gas-to-particle conversion. [15].

Chapter 2

Literature review

2.1 ZnO thin films

ZnO thin films deposited by sol-gel method using spin coating technique has been widely studied. Sahal et al. have studied this in their paper [16]. Transparent and high conductive thin films have been prepared using this technique. They doped Al in this and observed that higher the percentage of Al doped, lesser the resistivity obtained. Ziaul Raza Khan et al. [17]have deposited ZnO thin films on quartz substrate by the same technique. They have used 0.8 M zinc acetate solution. The optical band gap energy of the thin films is found to be direct allowed transition 3.24 eV. Nanda Shakti and P.S. Gupta [18]in their paper have showed structural and optical properties of ZnO thin films prepared by sol-gel method. They have deposited ZnO thin films on quartz substrate with the post annealing at 400°C, 500°C and 600°C and observed the change in properties. Youssef Ammaih et al. [19] used the same technique for ZnO thin films. They have doped Al and observed that the bandgap increases from 3.21 to 3.273 by increasing the doping concentration from 2 % to 3 %. S. ILICAN et al. [20] have found polycrystalline of ZnO thin films using sol-gel spin coating . They have reported grain size in the range of 25-32 nm. The interesting thing about this paper is that they have calculated I-V characteristics of ZnO thin films in dark and under UV light. Results showed that ZnO thin films are sensitive to UV light and hence can be used as window materials in photovolatic applications.

There has been many research going on in the research field of ZnO thin film preparation by spraypyrolysis technique. Shashidhara Bhat et al. [21]have prepared ZnO thin films on glass substrate. These glass substrates had been ultrasonically cleaned before deposition. The precurson solution was prepared using 0.1 M zinc acetate hexahydrate dissolved in mixture of 3:1 isopropyl alcohol and de-ionised water. A small amount of acetic acid was added to increase solubility of Zinc acetate. Hexagonal wurzite type polycrystalline type of ZnO were reported. Nadia Chahmat et al. [22] reported to have prepared ZnO thin films by spray pyrolysis technique using 0.1 M zinc acetate. They kept the temperature of substrate at 300°C while deposition. ZnO showed polycrystalline structure with (002) preferrential orientation.

Erdal Sonmez et al. [23] have used $ZnCl_2$ as a precursor for the synthesis of ZnO thin films. They have used spray pyrolyysis technique. They have calculated the bandgap of ZnO thin films to be 3.35 eV. Ankit Goyal and S. Kachhwaha in their paper [24] have

showed that they have prepared ZnO thin films using $ZnCl_2$ as a precursor. They have used 0.4 M of $ZnCl_2$ in 200 ml distilled water. They have reported to have obtained ZnO thin films of uniform grain size.

2.2 $BiFeO_3$ thin films

Annapu Reddy Venkateswarlu et al. [25] have deposited nano-crystalline BiFeO3 films using spray pyrolysis technique. They have used ultra cleaned glass as substrate. Their precursor consists of Bismuth nitrate (5% excess) dissolved in acetic acid and 2-methoxy ethanol (2:3) at room temperature and to it iron nitrate was added. Thin films have been deposited in the temperature ranges 200,300,400 °C and their properties have been compared. D J Huang et al. [26] have prepared BiFeO3 films on silicon substrates using spin coating. In their procedure they have used Bismuth nitrate, iron nitrate and lanthanum nitrate and these are dissolved in glacial acetic acid . Bismuth nitrate should be 5% excess. Ethylene glycol was also added to adjuct stickiness of the precursor. The films hance obtained are uniform and crack-free. C. Himcinschi et al. [27] have developed BFO thin films using pulsed laser deposition. They have basically studied the substrate influence on optical and structural properties of BFO thin films deposited by pulsed laser deposition. Results showed presence of larger compressive strain for BFO deposited on STO ($SrTiO_3$) with respect to DSO($DyScO_3$) .

2.3 Multi layer thin films

BFO has been widely used in multilayer thin films. Seo-Hyeon Jo et al. [28] have studied electrical properties of PZT/BFO multilayer thin films. Thin films have been prepared by spin coating. After three to five layers of deposition thin film system was void free and uniform. The grain size was inversely propertional to the number of layers. The reason they stated was that lower layers act as nueclon site or seed layer for the formation of uniform upper layers. Dielectric loses decreased with the increase in number of layers. The interface between PZT and BFO act as sinks for layers. However, they suggested more investigation for the full understanding of the charge distribution at the interface of PZT and BFO thin film layers. Z.-H.Wang et al. [29] have studied multiferroic properties of BiFeO3/Co/$BiFeO_3$ multi layer structure. They showed that BFO/Co/BFO multi layer structure changes from the antimagnetic to ferromagnetic phase with increasing thickness of Co layer.

Chapter 3

Synthesis

For the synthesis of thin films, a substrate is required. In this case of thin film deposition, glass is used as a substrate. Glass is used as a substrate as it has a smooth surface, low cost, stable upto 400°C , easy availability, insulating in nature and transparent. For our purpose, we used glass pieces of size 1 cm^2. For the cleaning of glass, ultrasonication mathod is used. Glass pieces are sonicated using acetone for 20 minutes. Then they are rinsed with DI water.

A home made spray pyrolysis method is used for fabrication of thin films. Electric heater is used to provide heat to warm the substrate to a required temperature. A solid uniform thermal conductor surface is neatly cleaned and heated. Cleaned glass slides are then placed on a solid uniform thermal conductor surface to provide proper and uniform heating to the substrate.

3.1 Synthesis of ZnO thin films

Zinc Oxide thin films are synthesized using Zinc Chloride as a precursor solution. 0.4M solution of anhydrous $ZnCl_2$ anhydrous is prepared in 100 ml distilled water. Before spraying, the glass slides were heated for 15 minutes. The precursor solution was sprayed at a rate of 15 psi. After spraying glass slides again heated for 10 minutes. Films on glass slides were sintered inside the Furnace. The sample is heated at a rate of 5°C per minute and is kept at 400°C for 1 hour.

3.2 Preparation of $BiFeO_3$ thin films

First of all precursor solution was prepared. 38 mL distilled water and 12 mL HNO_3 was mixed ,to it 0.005 M of $Bi(NO3)_3.5H_2O$ was added and this was kept in a beaker. In another beaker 0.005 M of $Fe(NO_3)_3.9H_2O$ and 50 mL of water was mixed. In another beaker 0.7507 g.m. of glycine was taken and to it the contents of the beaker prepared previously was added. This solution was used as a precursor. Before spraying the glass slides were heated for 15 minutes. The precursor solution was sprayed at a rate of 15 psi. After spraying glass slides again heated for 10 minutes. Films on glass slides were sintered at 400°C for 1 hour inside the Furnace.

Figure 3.1: Home made spray pyrolysis setup

3.3 Preparation of multi-layer thin films

Multi layer thin films were prepared by layer by layer growth of thin films by spray pyrolysis technique. Individual layers were deposited using the same technique as above. Before the deposition of every layer except the first, the thin films were sintered at 400°C. So for the synthesis of ZnO-BFO thin film, first Zno thin film was prepared. After that it was sintered at 400°C and after that $BiFeO_3$ was deposited on it.

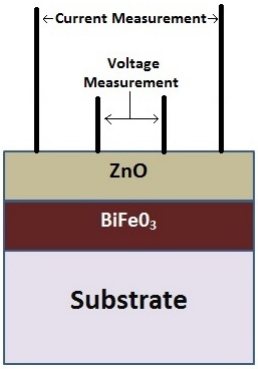

Figure 3.2: Schematic diagram of BFO/ZnO multilayer thin film

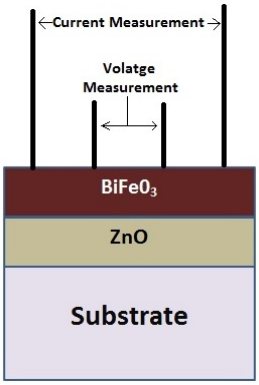

Figure 3.3: Schematic diagram of ZnO/BFO multilayer thin film

3.4 Preparation of BFO-ZnO thin film junction

For the preparation of BFO-ZnO thin film junction the following procedures have been employed. First ZnO thin films are prepared on the glass substrate as shown in the figure. In this case more than half of the surface area of the substrate is exposed to the spray of ZnO precurser. Other areas are masked with the help of aluminium foil. After the spray of ZnO precurser, Again the a mask is given on the surface of the substrate as follows. It is made sure that the BFO precurser would be sprayed on glass as well as some areas of ZnO thin film. Finally, the sample is sintered at 400°C.

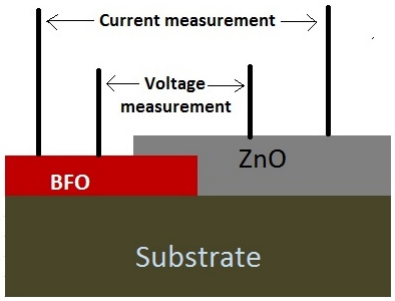

Figure 3.4: Schematic diagram of BFO-ZnO junction

Chapter 4

Characterization techniques

4.1 X-Ray diffraction

This method is helpful in finding various information about the crystalline nature of the sample. These information may be the lattice structure, phase composition, crystalline nature(crystal or amorphous). X-rays fall on the sample and the diffraction occurs when Braggs condition is satisfied.

$$n\lambda = 2dsin\theta$$

Here, n = orader of diffraction,
d = interplanner spacing,
λ = wavelength of the incident beam,
θ = angle of diffraction
The intensity of diffracted X-rays are plotted against scattering angle. Analysing the peaks gives us possible information.

4.2 Field Emission Scanning Electron Microscopy

This method has been widely used in material characterization to study morphology and topological features. Unlike SEM, this method used high potential to generate electron beam. Being accelerated through a high potential, electrons attains less wavelength and hence the resolution of image increases significantly. There are various electromagnets inside the setup to control the electron beam falling on the specimen surface. Various particles like secondary electrons, backscattered electrons come out of the sample due to the interaction of the specimen with the specimen. These particles carry different kind of information.

4.3 UV-Vis Spectroscopy

UV-Visible spectroscopy uses wavelength ranges from 200 to 900 nm i.e. from UV to visible light range to study transmittance, reflectance and absorbance spectra of materials. Transmittance spectra can be used to calculate the band-gap of the material. Reflectance spectra can be used to find the thickness of the material. Band Gap of a semiconductor

can be measured using UV-Visible spectroscopy by following relation

$$(\alpha h\nu)^{\frac{1}{n}} = B(h\nu - E_g)$$

Where,
Absorption Coefficient $\alpha = -log(T)/(d)$
T = Transmittance
d = Thickness of the film
n = 2 Indirect band Gap, $\frac{1}{2}$ Direct Band Gap
B = Constant related to transition probability

4.4 I-V Measurement

I-V characteristic of a circuit is generally used to find the impedance of the circuit and the junction property. There are basically two type of contacts. They are Ohmic contacts and Schottky contacts. While Ohmic contacts show a linear graph, Schottky contacts show a nonlinear graph for the I-V measurement. This method is very helpful in analysing the characteristics of various materials such as semiconductors, MOSFET etc.

4.5 R-T Measurement

Temperature dependence of resistivity is one of the techniques to know the conducting nature of the sample. Different type of materials would show different nature of graphs hence classifying themselves as metals, semiconductors or insulators. There are 2 type of measurement can be done with the circuit.

- Four probe method
- Two probe method

Two probe method can be used for samples those have high resistance.

Different types of contacts are as follows

- Van der Pauw method
  This method is known for its accurate measurement of resistance of any shape, if it is two dimensional. The schematic diagram for this method is as follows. Alternate contacts are taken for voltage measurement. SImilarly, alternate contacts are taken for current measurement.

- linear contact
  This method is used in some cases. The schematic diagram for this methis is as follows.
  Extreme end contacts are taken for voltage measurement and middle contacts are taken for current measurement.

For the contact, silver paste has been used. After putting the silver epoxy, the sample was heated under a warm lamp for about 4 hours. Doing so gives a good adhesion between the contact and the sample. After the double sided tape is applied, the sample

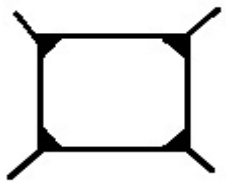

Figure 4.1: Van der Pauw contact

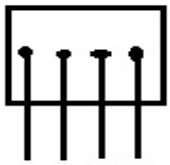

Figure 4.2: Linear contact

was mounted, the system was kept under vacuum condition by a vacuum pump. After the vacuum condition is achieved, the measurement of resistance with temperature is started. In these processes, first the sample is cooled and then after reaching a desired low temperature, the sample is heated. And hence, the R-T nature of the sample in both heating and cooling conditions is achieved. The resistivity measurement is done with the help of electrometer (Keithely 6517B). All the instruments are interfaced to a personal computer via IEEE interfacing card. A computer program is written using Labview software, to collect the data from the instruments.

For the calculations where a magnetic field is to be applied, a magnetic field of 1 Tesla is applied with the help of electromagnets.

4.5.1 Magnetoresistance

Magnetoresistance is the property of a material by which its electrical resistance changes due to the application of an external field. Some materials show a higher percentage of magnetoresistance of orders of magnitude. The percentage of magnetoresistance is

calculated as,

$$\frac{R_M - R_0}{R_0} \times 100$$

4.5.2 Arrhenius equation

Most materials follow a temperature dependance of resistance behavior which is governed by an Arrhenius equation over a wide range of temperatures:

$$R = R_0 e^{-E_a/T}$$

$$lnR = lnR_0 - \frac{E_a}{T}$$

where R is the resistance, T is the temperature (K) E_a is the activation energy. By plotting ln R in the y- axis and $1/T$ in the x-axis and by calculating the slope, we would get activation energy E_a

As the value of activation energy(E_a) increases, the material becomes insulating.

4.5.3 Variable-range hopping

Low-temperature conduction in strongly disordered systems in which there are localized charge carrier states can be explained by Mott's variable-range hopping.[30]

It has a characteristic temperature dependence of

$$\rho = \rho_0 e^{-(T_M/T)^{1/4}}$$

[31] where T_M is the parameter called Mott temperature

$$ln(\rho) = ln(\rho_0) - (T_M/T)^{1/4}$$

Linearly fitting $ln(\rho)$ with $T^{-\frac{1}{4}}$, we would get the Mott temperature.
Semiconductor industries are interested in replacing single-crystal devices with glass layers because of the savings they would make. That's why hopping conduction at low temperature is of great interest.[32]

Chapter 5

Results and Discussions

5.1 ZnO thin films

5.1.1 XRD Analysis

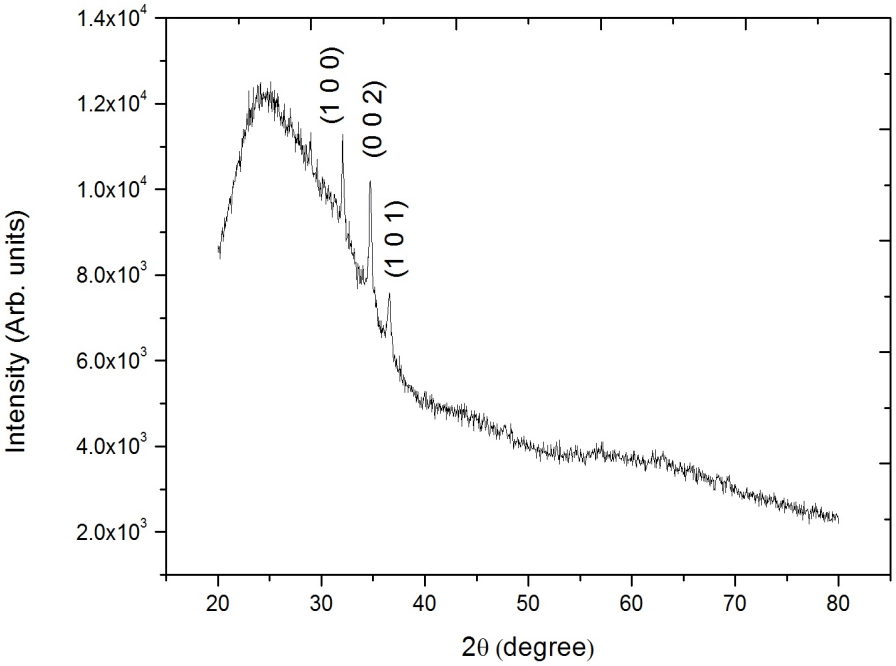

Figure 5.1: XRD image of ZnO thin film

X-ray diffraction pattern of zinc oxide thin film on glass substrate. The numerals inside the brackets are the respective (hkl) planes.

- XRD peaks are indexed depending on their space group (S.G.).
- No secondary phases are observed.
- The structure of ZnO formed is hexagonal structure.

5.1.2 UV-Vis analysis of ZnO thin film

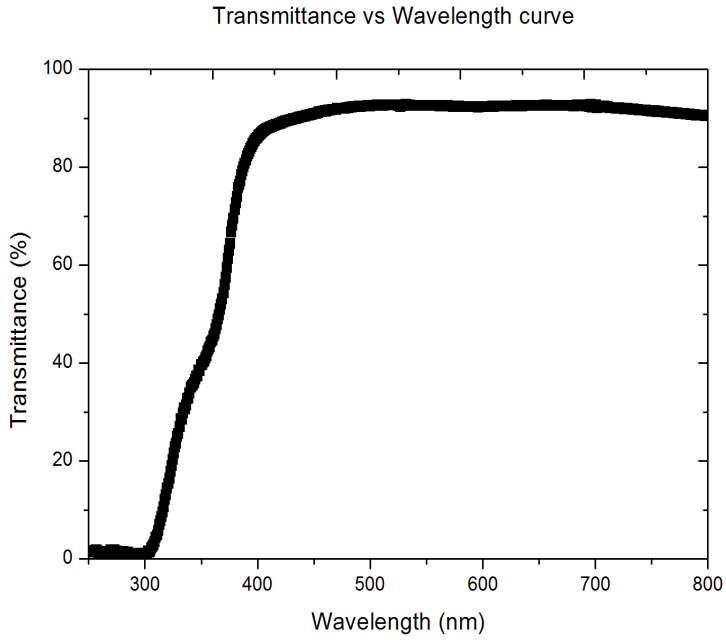

Figure 5.2: UV-Vis spectroscopy of ZnO thin film

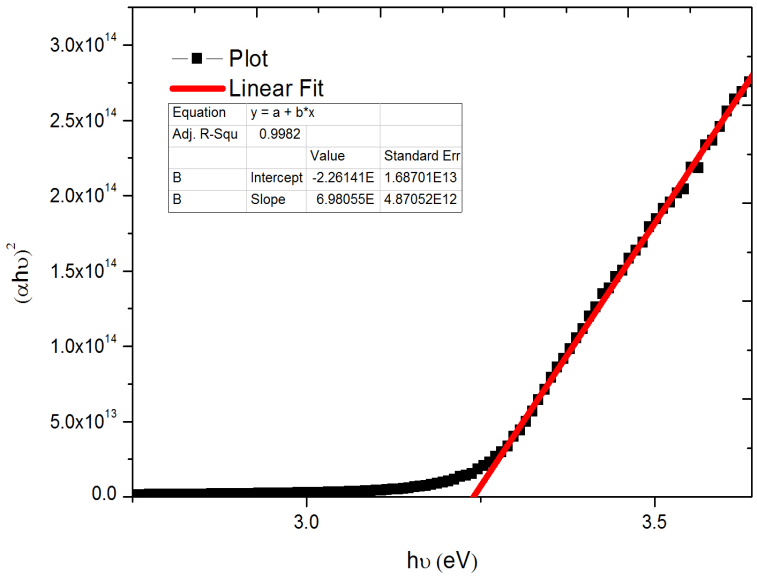

Figure 5.3: Bandgap calculation graph of ZnO thin film

The bandgap of ZnO thin film is found to be 3.24 eV. ZnO has a direct bandgap of 3.37 eV.

5.1.3 FESEM analysis of ZnO thin film

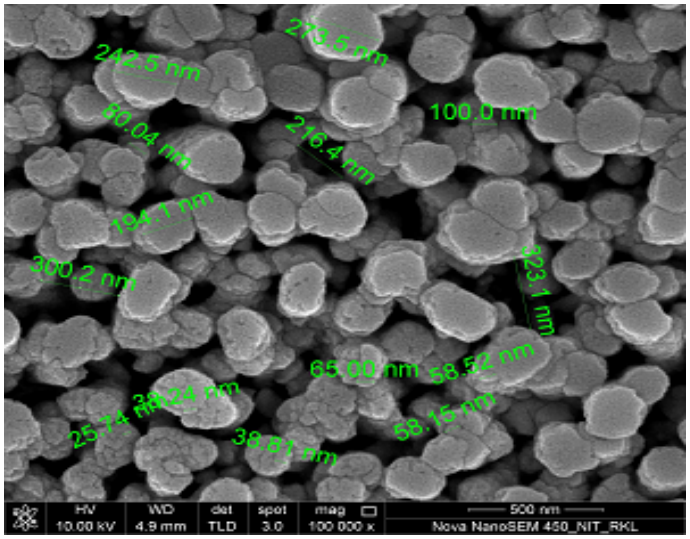

Figure 5.4: FESEM image of ZnO thin film

From this picture, as we are seeing some porosity, we can use this in the case of gas sensors. From the FESEM analysis of ZnO thin films, it is found that there exists different grain sizes. However, there grains may be characterized in two sets, smaller grains and larger grains. Again, small grains are agglomerated to develop a larger grain. Larger grains are also uniform like smaller grains. Smaller grains of size 25-100 nm have been found within larger grains of size 200-300nm.

5.1.4 R-T measurement of ZnO thin film

An experimental setup was designed to study R-T behavior of samples. In this procedure liquid nitrogen has been used as coolant. From this graph, it can be noted that with

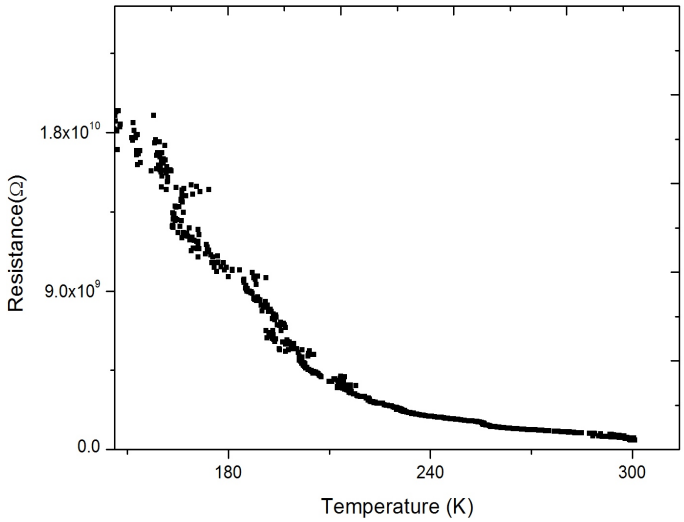

Figure 5.5: R-T measurement of ZnO thin film

decrease in temperature, resistance of this material increases.

5.2 BFO thin film

5.2.1 XRD Analysis

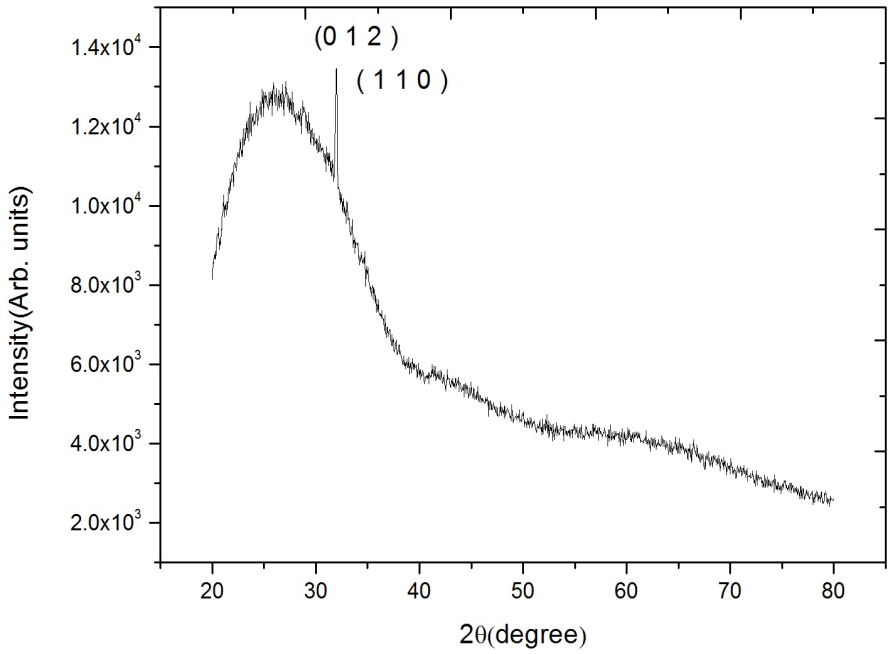

Figure 5.6: XRD graph of BFO thin film

X-ray diffraction pattern of BFO thin film on glass substrate. The numerals inside the brackets are the respective (hkl) planes.

- XRD peaks are indexed depending on their space group (S.G.).
- No secondary phases are observed.
- The structure of BFO formed is rhombohedral.
- Single peak of BFO suggests the growth of the film in either (1 1 0) or (0 1 2)plane direction.

5.2.2 UV-Vis analysis

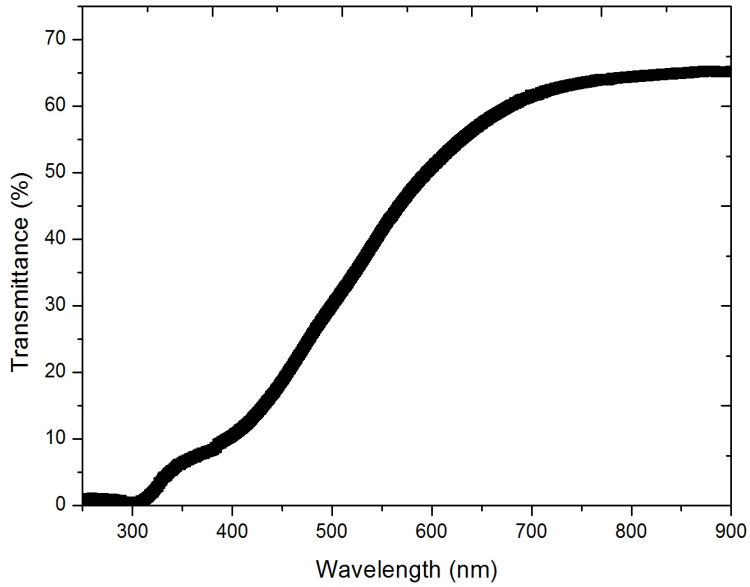

Figure 5.7: UV-Vis spectroscopy graph of BFO thin film

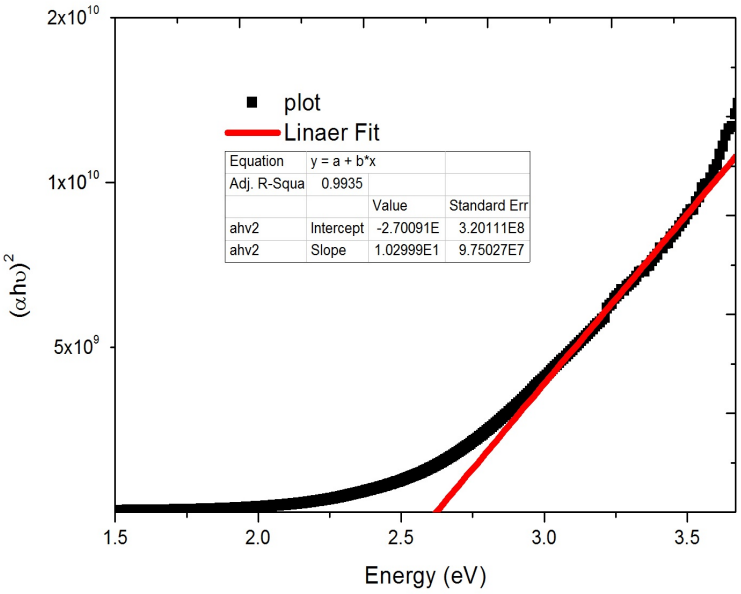

Figure 5.8: Bandgap calculation graph of BFO thin film

The bandgap of BFO thin film is calculated to be 2.62 eV. Its value from literature review was found out to be 2.67 eV.

5.2.3 FESEM analysis

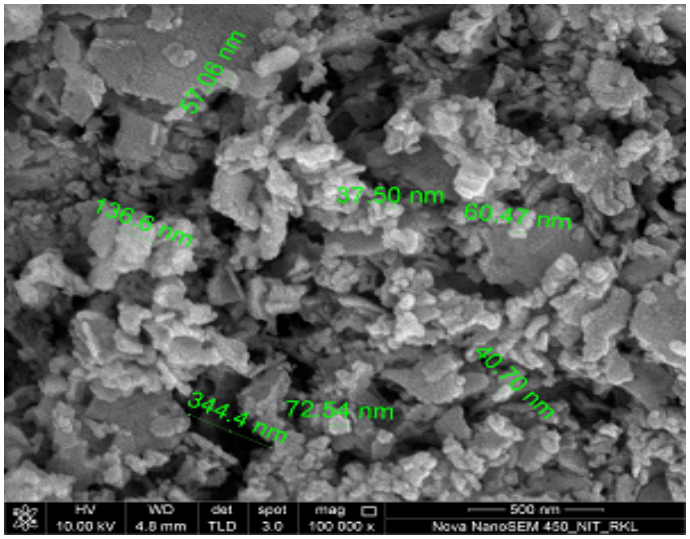

Figure 5.9: FESEM inage of BFO thin film

The grain size from this experiment is found out to be 37-137nm

5.2.4 R-T measurement of BFO thin film

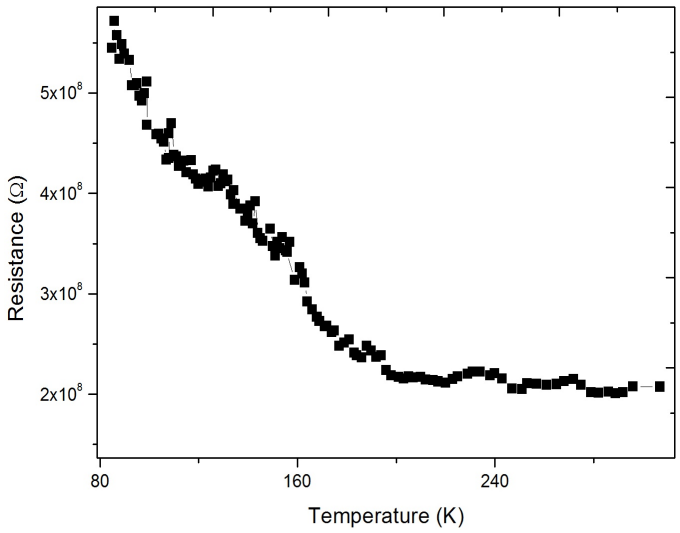

Figure 5.10: R-T measurement of BFO thin film

5.3 BFO/ZnO multilayer

5.3.1 UV-Vis analysis

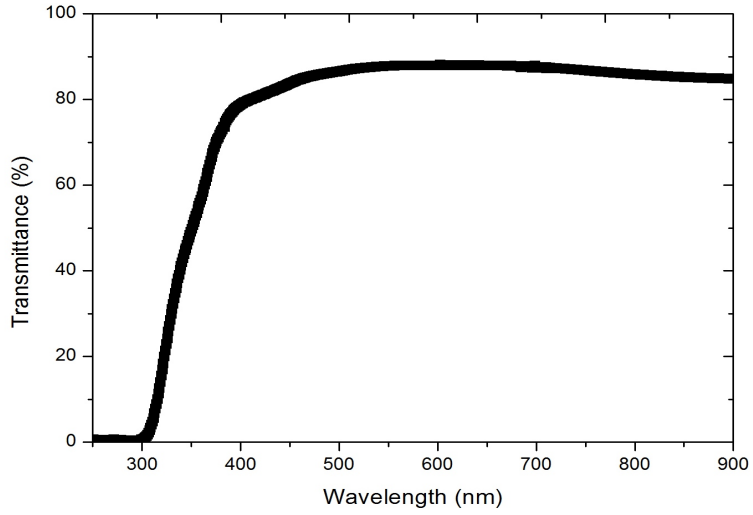

Figure 5.11: UV-Vis spectroscopy graph of BFO/ZnO multilayer

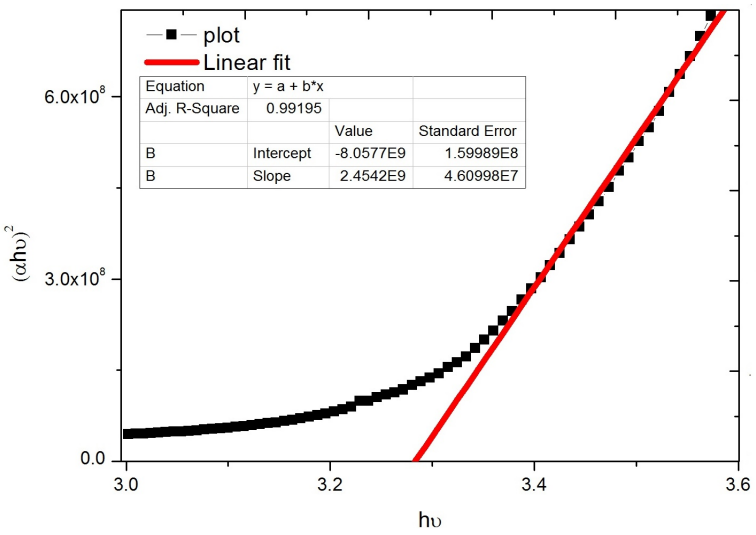

Figure 5.12: Bandgap calculation graph of BFO/ZnO multilayer

The bandgap is found out to be 3.28 eV.

5.3.2 FESEM analysis

From FESEM analysis, it is found that grain size of 30-40 nm are present in the sample. Ocassionally, there are some particles with anamoly shape are found. These shapes are mostly Rectangular cuboid.

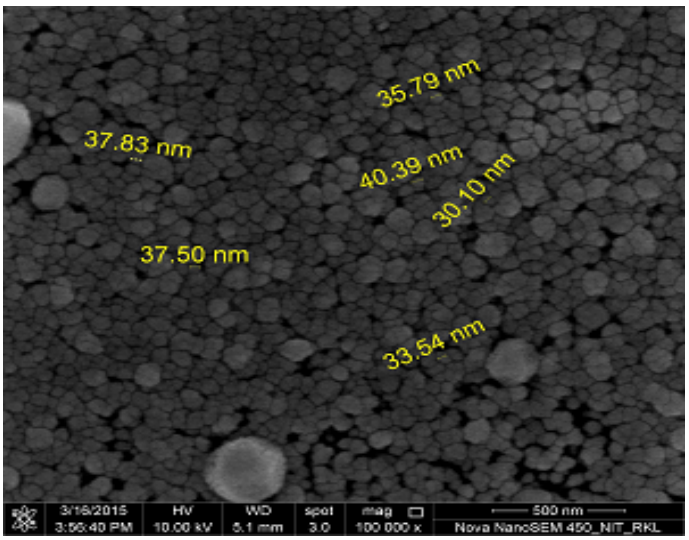

Figure 5.13: FESEM image of BFO/ZnO multilayer-1

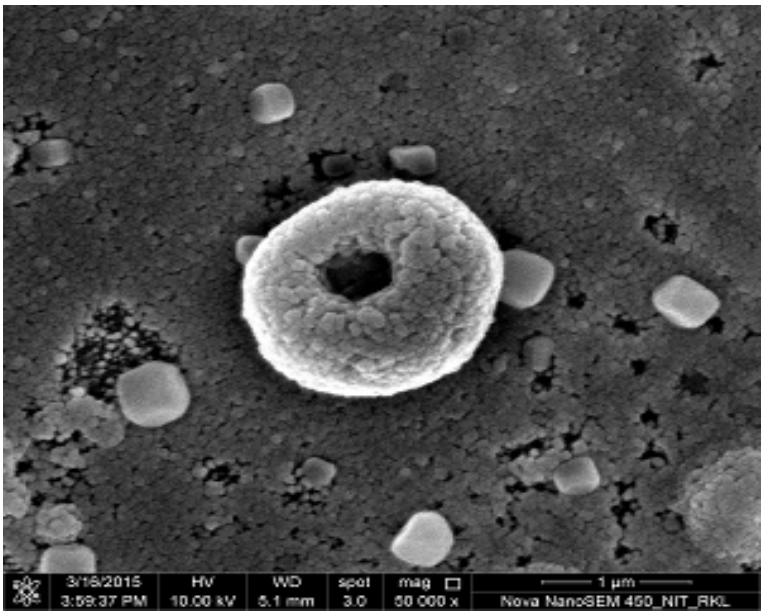

Figure 5.14: FESEM image of BFO/ZnO multilayer-2

5.3.3 R-T measurement

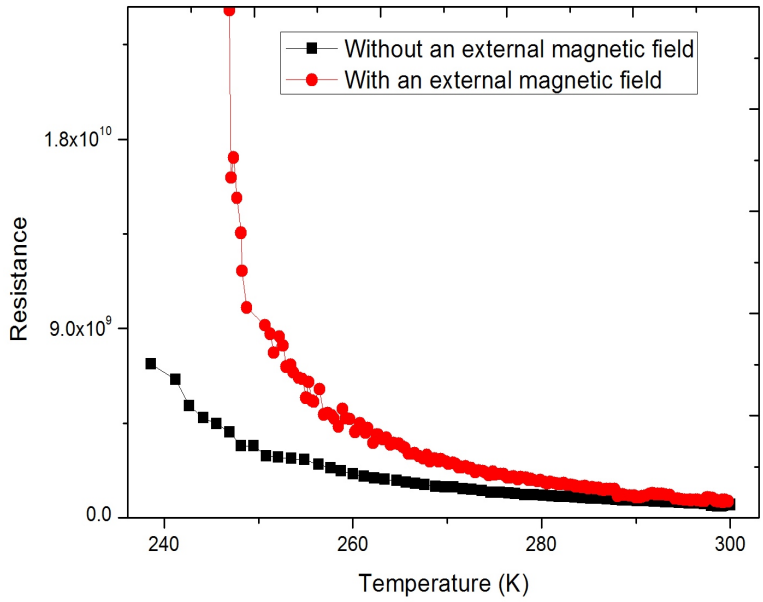

Figure 5.15: R-T measurement of BFO/ZnO multilayer

From the R-T measurement of BFO/ZnO multilayer it is observed that the resistance of the system increases with the decrease in temperature. By the application of an external magnetic field of 1 Tesla, the resistance further increased. From the % magnetoresistance graph, it is observed that the % magnetoresistance increases with the decrease in temperature. Magnetoresistance of approximately 300 % has been observed

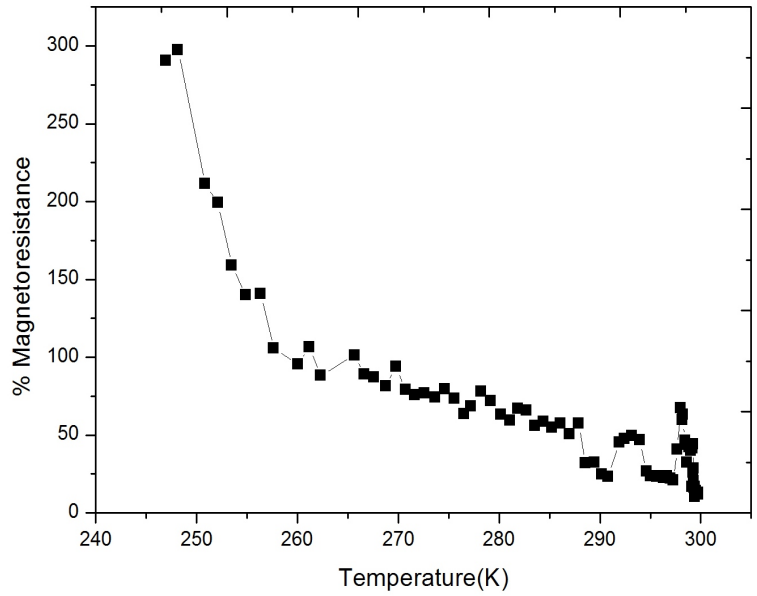

Figure 5.16: % Magnetoresistance of BFO/ZnO multilayer

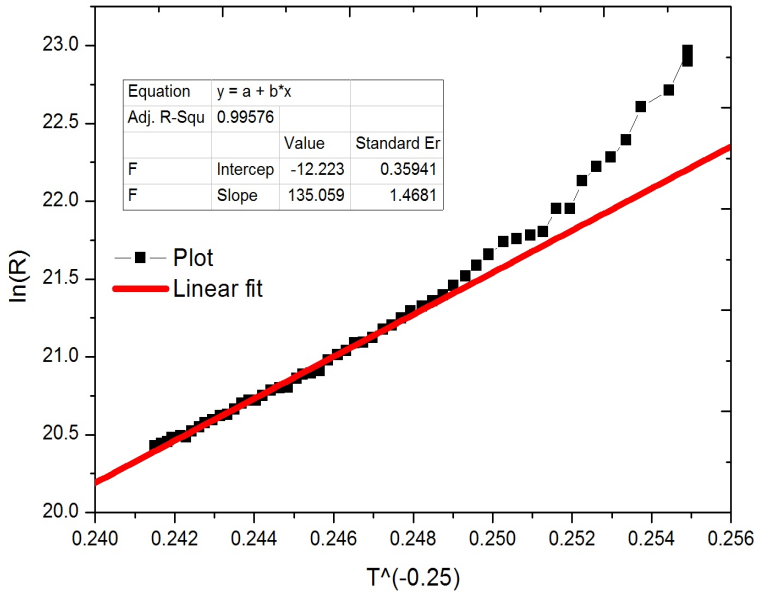

Figure 5.17: lnR Vs. $T^{-\frac{1}{4}}$ without external magnetic field

for temperature approximately 250 K. This material does not follow Arrhenius equation. It rather follows Mott's VRH for certain temperture ranges.

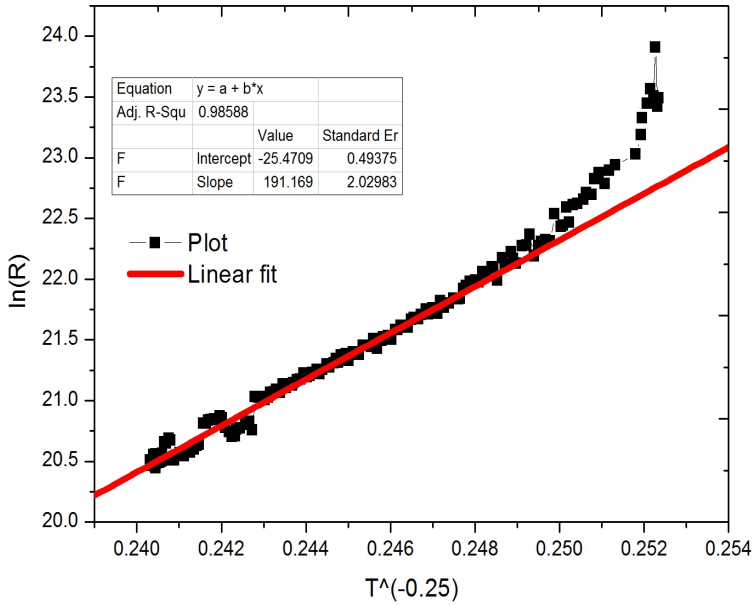

Figure 5.18: lnR Vs. $T^{-\frac{1}{4}}$ with an external magnetic field

After applying an external magnetic field, this material still shows a good fit to the Mott's VRH. However, while the Mott's temperature of this material was $(135.059)^4)$K, it was $(191.169)^4)$K after an external magnetic field of 1 Tesla is applied.

5.3.4 I-V measurement

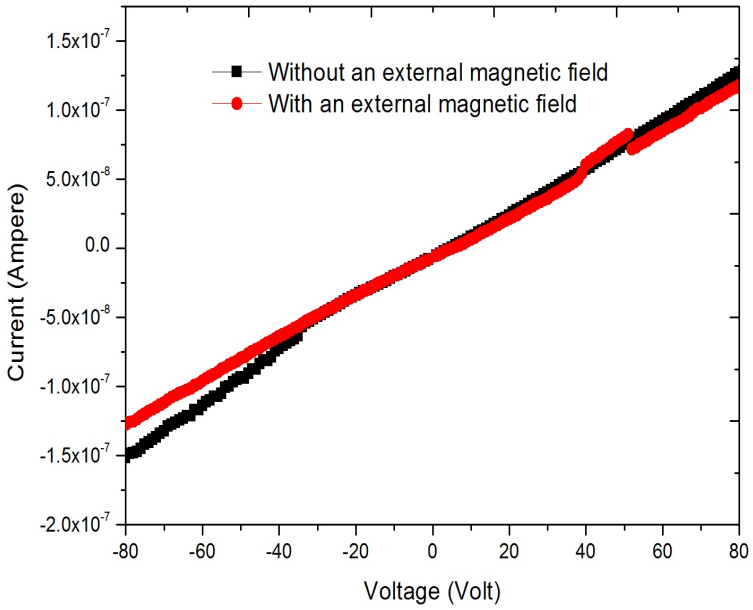

Figure 5.19: I-V measurement of BFO/ZnO multilayer

The I-V graph in this case is linear. Some variation in the I-V graph has been observed after an external magnetic field is applied.

5.4 ZnO/BFO multilayer

5.4.1 UV-Vis analysis

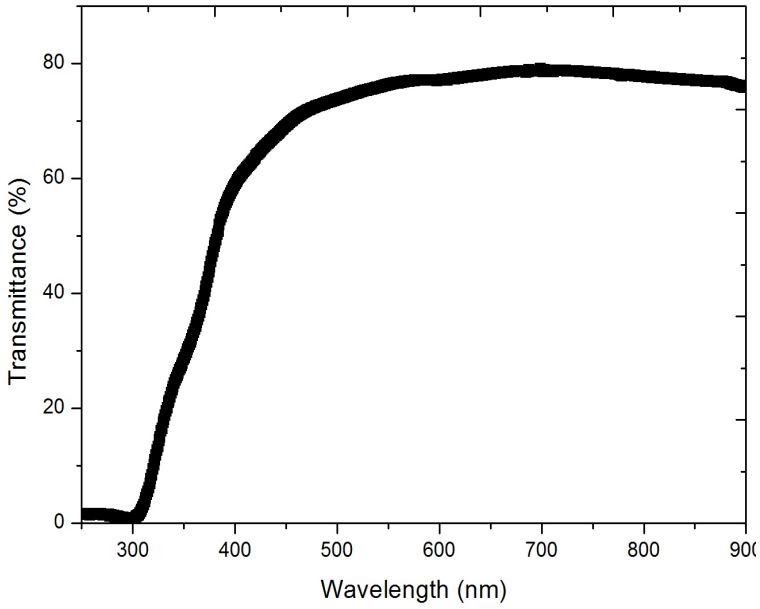

Figure 5.20: UV-Vis spectroscopy graph of ZnO/BFO multilayer

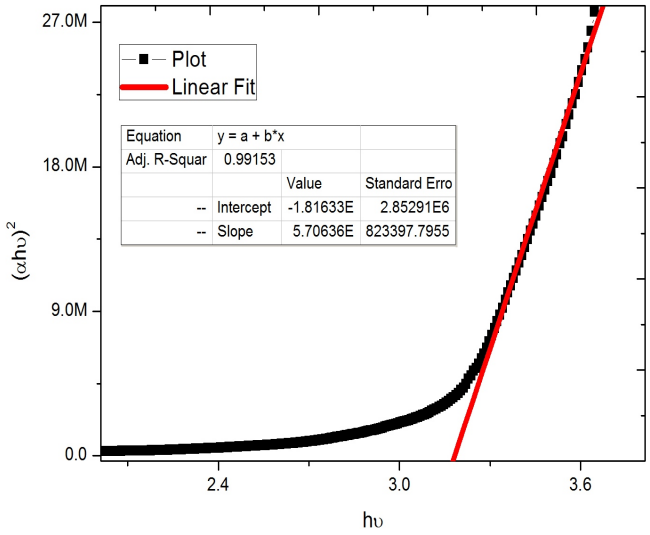

Figure 5.21: Bandgap calculation of ZnO/BFO multilayer

The bandgap was found out to be 3.19 eV.

5.4.2 FESEM analysis

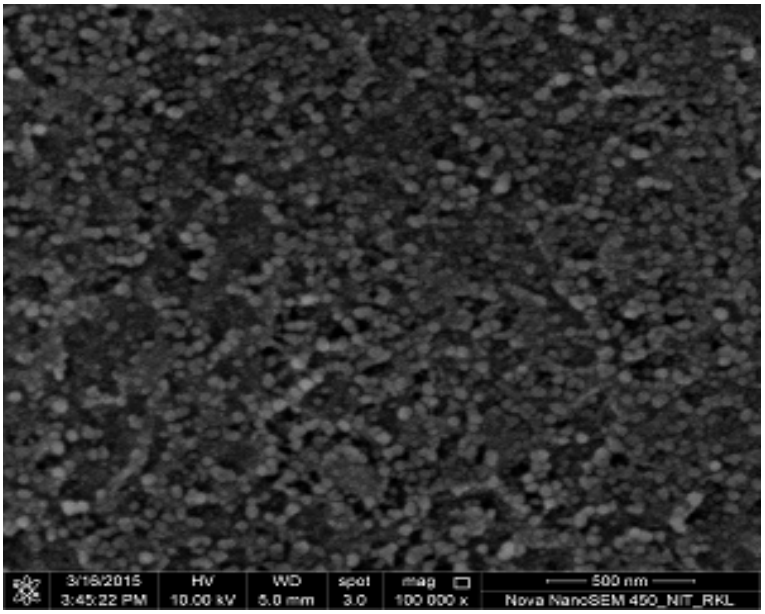

Figure 5.22: FESEM image of ZnO/BFO multilayer

Uniform grains are observed. This structure have less porosity.

5.4.3 R-T measurement

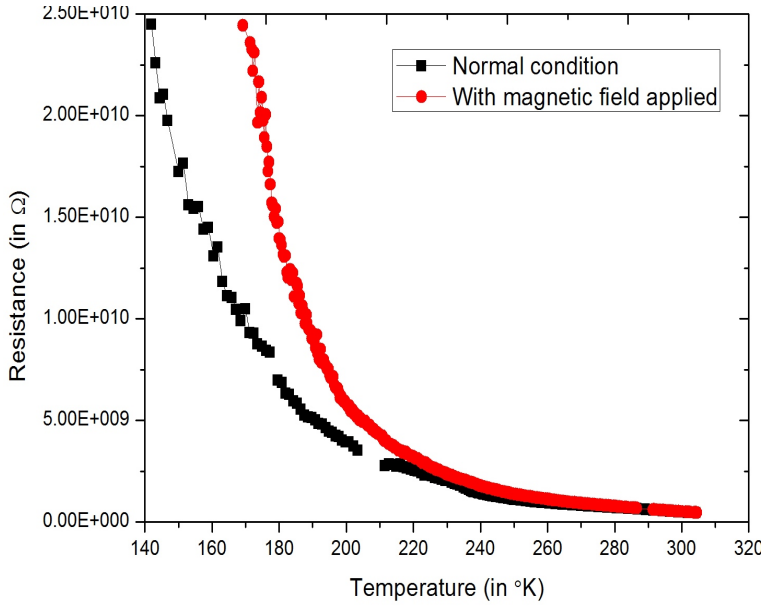

Figure 5.23: R-T graph of ZnO/BFO multilayer

With the decrease in temperature, the resistance of the sample increases. This means that this multilayer shows a negative temperature coefficient. This negative temparature

coefficient increases with the application of an external magnetic field, which in this case is 1 Tesla.

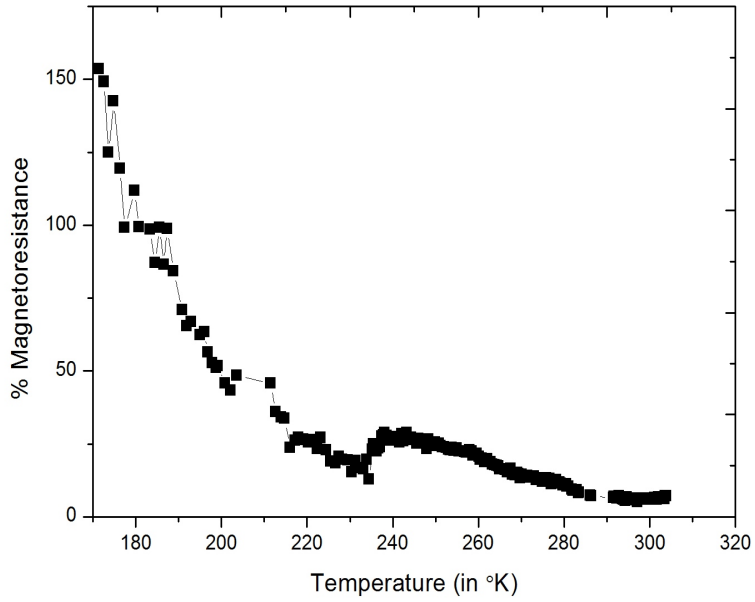

Figure 5.24: % Magnetoresistance of ZnO/BFO multilayer

Magnetoresistance: The magnetoresistance in different temperatures has been found out to be as per the following graph. From this graph it is found out that as we decrease the temperature the percentage of magnetoresistance increases. This multilayer shows a high percentage of magnetoresistance (150%) in the approximate temperature of 170 K.

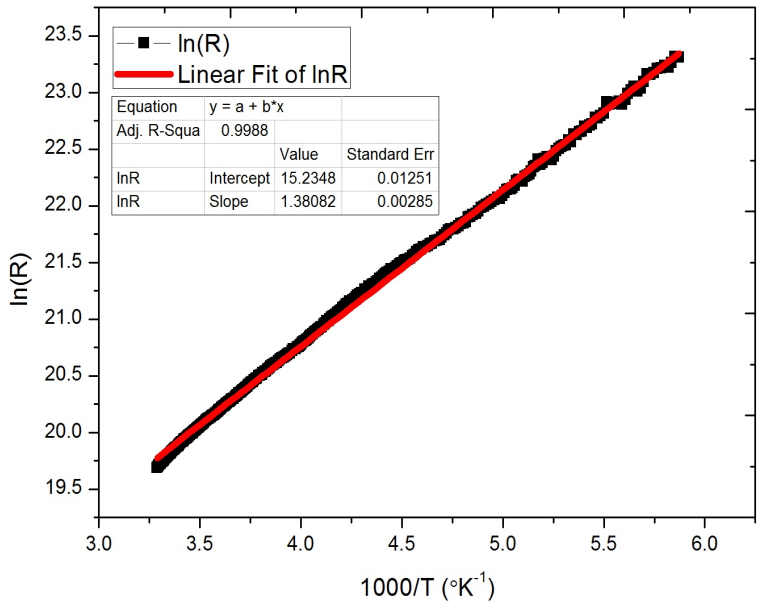

Figure 5.25: Calculation of Activation energy without magnetic field applied

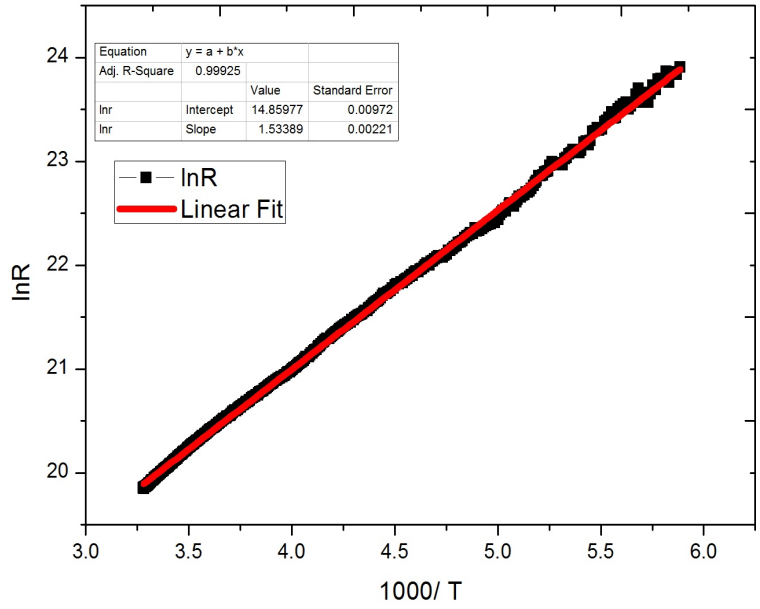

Figure 5.26: Calculation of Activation energy with magnetic field applied

This material shows a netgative temperature coefficient and follws Arrhenius equation as found out from the graph. It shows a perfect fit to the Arrhenius equation. While in normal conditions it showed an activation energy of 1.38eV, it was 1.53eV in the case when a magnetic field is applied.

5.4.4 I-V measurement

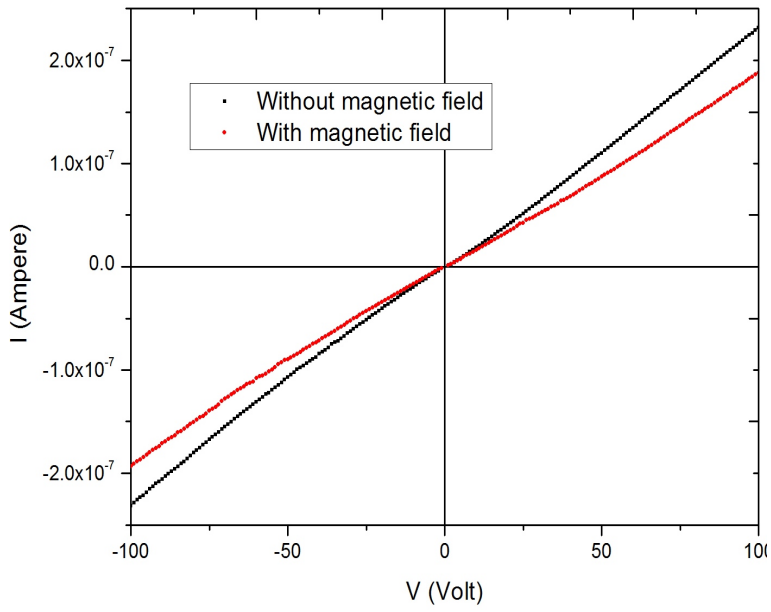

Figure 5.27: I-V graph of ZnO/BFO multilayer

This multilayer system shows a linear behavior in the I-V characteristics graph. How-

ever when a magnetic field of 1 Tesla is applied, the I-V graph showed a different slope as the resistance changed.

5.5 BFO-ZnO junction

5.5.1 R-T measurement

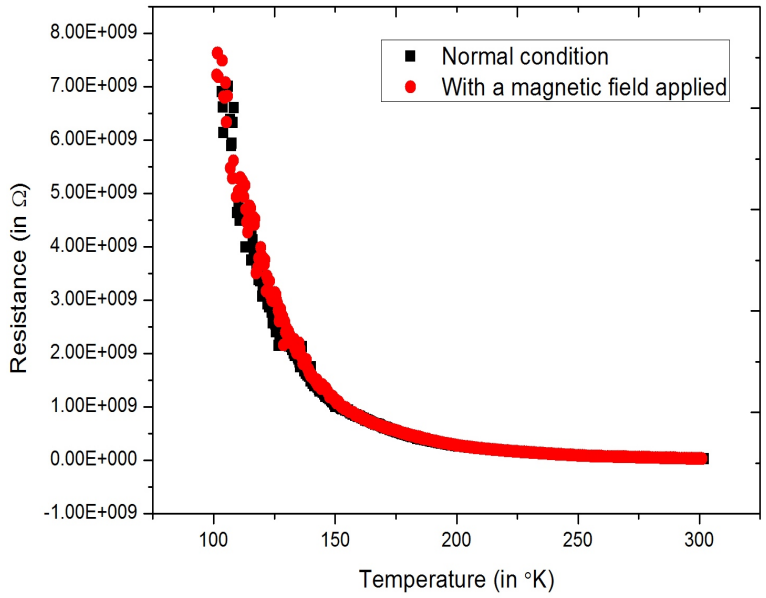

Figure 5.28: R-T graph of BFO-ZnO junction

From this graph, it is clear that this material shows a negative temperature coefficient for resistance as with the decrease in temperature, the resistance of the material increases. Application of an external magnetic field shows little effect on the R-T behavior. Both the graphs (with and without magnetic field) follows almost same path in the R-T graph.

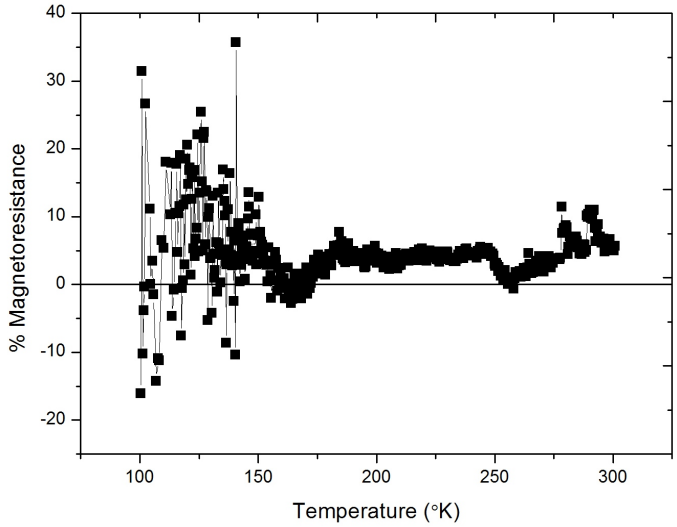

Figure 5.29: % Magnetoresistance of ZnO BFO junction

The magnetoresistance calculated and plotted for this sample shows almost a flat curve with the % MR almost always less than 10%.

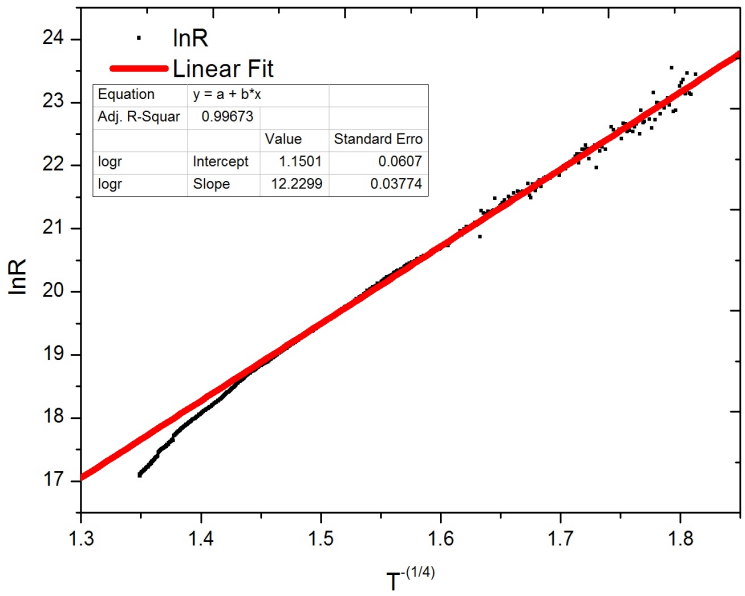

Figure 5.30: lnR Vs. $T^{-\frac{1}{4}}$ without external magnetic field applied

This material does not follow Arrhenius equation. However, it shows a perfect fit with Mott's VRH for a large temperature range. With the application of magetic field, this

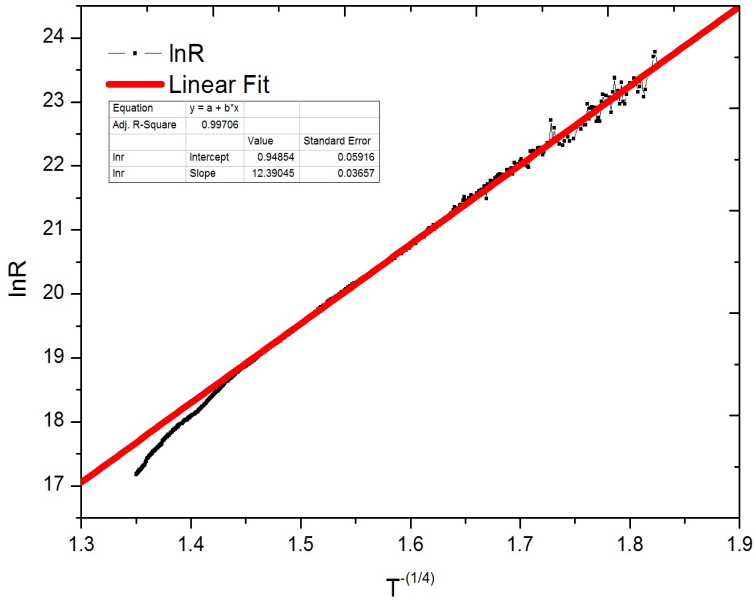

Figure 5.31: lnR Vs. $T^{-\frac{1}{4}}$ with external magnetic field applied

material again shows a good fit with the Mott's VRH. While the Mott's temperature in the previous case was $(12.23)^4K$, it was $(12.39)^4K$ after a magnetic field of 1 Tesla is applied.

5.5.2 I-V Measurement

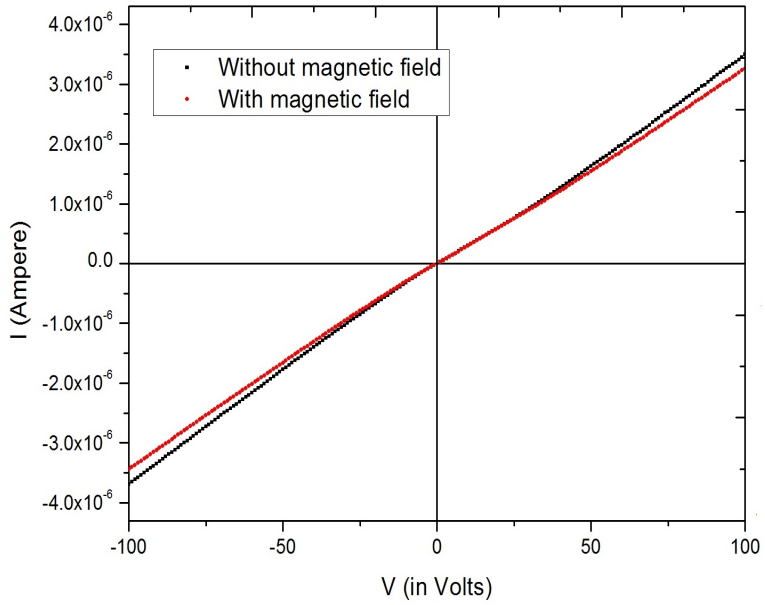

Figure 5.32: I-V graph of BFO-ZnO junction

This system shows a linear behavior in the I-V graph. However, when an external magnetic field of 1 Tesla is applied, it showed a different slope because of the change in resistance.

Chapter 6

Conclusion

ZnO thin film were prepared by spray pyrolysis method. No secondary phases are observed in the XRD analysis. The bandgap of the obtained thin film is found out to be 3.24 eV. The grain size is found out to be of 200-300 nm inside which smaller grains of size 25-100 nm has been observed. Due to the porosity observed in this thin film, this can be used in gas sensors.

BFO thin film has been synthesized using spray pyrolysis and is confirmed from the XRD analysis. From XRD analysis, it is also found out that there is a directional growth of BFO thin film. The bandgap of BFO thin film is found out to be of 2.62 eV. The grain size is found out to be of 37-137nm.

In BFO/ZnO multilayer, the bandgap is found out to be of 3.28 eV. From FESEM analysis, it is found that grain size of 30-40 nm are present in the sample. Ocassionally, there are some particles with anamoly shape are found. These shapes are mostly rectangular cuboid. In this material, with the decrease in temperature, resistance increases rapidly. A approximate 300% magnetoresistance has been observed in 248 K. BFO/ZnO follows Mott's VRH. With the application of 1 Tesla magnetic field, mott's temperature changes from approximate $(135)^4$K to approximate $(191)^4$K.

In the case of ZnO/BFO multilayer, the bandgap is found out to be of 3.19 eV. Grains of uniform size have been observed from the FESEM analysis. From the R-T measurement it is found that as the temperature decreases, the resistance of the material increases rapidly. With the application of an external magnetic field, this increase in resistance further increases. From magnetoresistance graph it is found out that the percentage of magnetiresistance increases by 150% at a temperature 170 K. This material follows Arrhenius equation for resistance with respect to temperature. The activation energy is found out to be of 1.38 eV , which increases to 1.53 eV when an external magnetic field of 1 Tesla is applied. The I-V graph of this multilayer system follows a linear behavior.

Considering the bandgaps of thin films and multilayers thin films, we can observe the following. The bandgap of ZnO thin film increases if it is deposited on a BFO thin film instead of directly on glass. However, to decrease the bandgap of ZnO thin films, we can deposit a BFO layer on it. Here, we should note that the bandgap of ZnO is greater than bandgap of BFO.

In the case of BFO-ZnO junction, the resistance increases with the decrease in temperature. With the application of an external magnetic field, there is not much variation is observed. The magnetoresistance graph showed an almost flat curve of % magnetoresistance of less than 10 %. This ZnO-BFO junction does not follow an arhenius type of behavior. Rather it follows Mott's variable-range hopping graph. It has a good fit with Mott's VRH for a wide range of temperature. The Mott's temperature for this sample is found out to be of $(12.23)^4$K which changes to $(12.39)^4$K when an external magnetic field of 1 Tesla is applied.

A comparison between the R-T measurement graphs in the conditions of without and with the application of an external magnetic field is as follows.

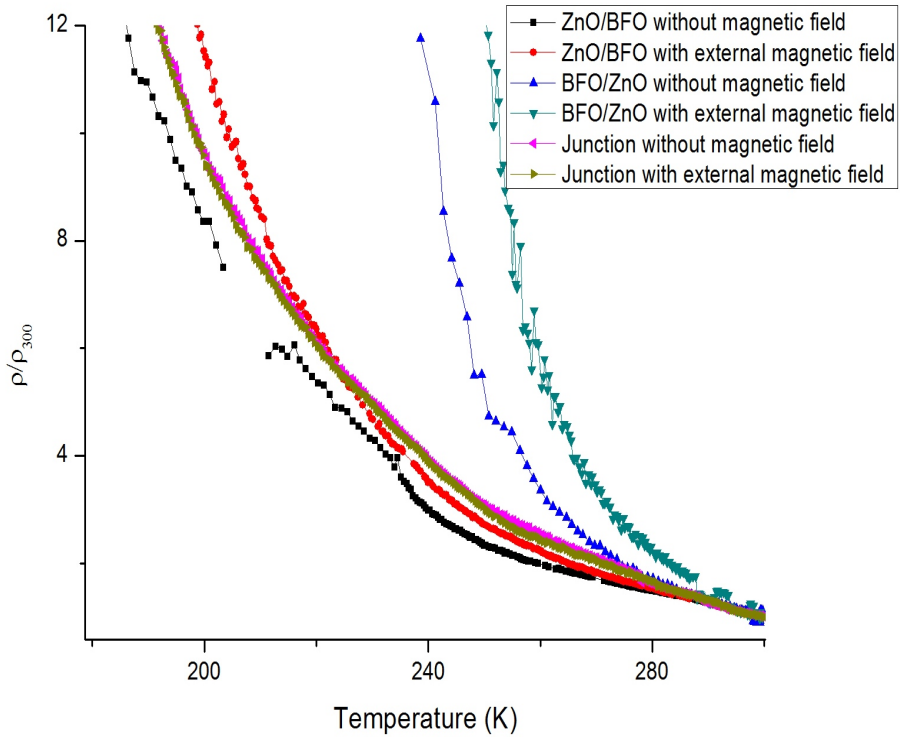

Figure 6.1: comparision - 1

With the application of an external magnetic field, the resistance of multilayers increases. However, in the case of junction, application of an external magnetic field has very less effect on resistance. Hence, it can be concluded that the effect of an external magnetic field on the change of resistance occurs in the surface, not in the junction.

A comparison between the R-T measurement graphs between all five samples in the heating condition is as follows. The bandgap of the materials are mentioned with their R-T curve.

It should be noted that there is a correlation between the rise of resistivity and the

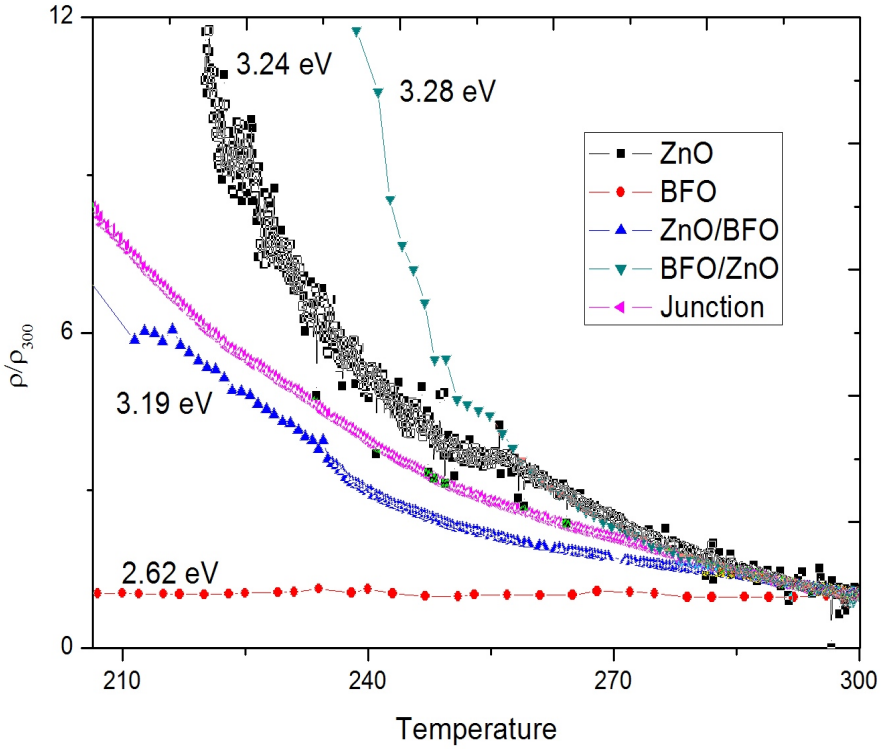

Figure 6.2: comparision - 2

bandgap of the material.

Bibliography

[1] WaghMS et al. Modified zinc oxide thick film resisters as gas sensor. *Sens Actuators B*, 115(1):12833, 2006.

[2] Litton CW Jones RL Eason DB Cantwell G. Look DC, Reynolds DC. Characterization of homoepitaxial p-type ZnO grown by molecular beam epitaxy. *Appl Phys Lett*, 81(10), 2002.

[3] Metal oxides: Chemistry applications. *CRC Press*, page 182, 2006.

[4] U Rossler. *Landolt-Bornstein, New Series, Group III.*, volume 17B, 22, 41B. 1999.

[5] Joydeep Dutta Sunandan Baruah. Hydrothermal growth of ZnO nanostructures. *Sci. Technol. Adv. Mater*, 10, 013001, 2009.

[6] R. P.; Kiselev, S. V.; Ozerov and G. S. Zhdanov. *International Journal of Materials, Mechanics and Manufacturing, Sov. Phys.*, 7:742, 1963.

[7] G.; Venevtsev, Yu. N.; Zhadanow and S. Solovev. *Sov. Phys. Crystallogr.*, 4:538, 1960.

[8] F.; Kubel and H. Schmid. Structure of a ferroelectric and ferroelastic mono domain crystal of the perovskite $BiFeO_3$. *Acta Crystallogr. B*, 46:698–702, 1990.

[9] I. P.; Fesenko. E. G.; Filipev, V. S.; Smolyaninov and I. I.; Kristallografiya Belyaev. 5:958, 1960.

[10] Hiroshi Naganuma Hiromi Shima and Soichiro Okamura. Optical properties of multiferroic $BiFeO_3$ films. *Materials Science - Advanced Topics*, 2013.

[11] David A. B. Miller Martina Gerken. Multilayer thin-film coatings for optical communication systems. *Optical Society of America*.

[12] E. Brsan. Magnetic properties of multilayer thin film with ising-like ordering. *Acta Physica Polonica A*, 117, 2010.

[13] C.-H. Solterbeck M. Es-Souni, S. Iakovlev. Multilayer ferroelectric thin films for pyroelectric applications. *Sensors and Actuators A*, 109:114119, 2003.

[14] C.Y. Chen et al. Effect of precursor characteristics on zirconia and ceria particle morphology in spray pyrolysis. *Ceram. Int.*, 2006.

[15] M.J. Hampden-Smith T.T. Kodas. Aerosol processing of materials. *Wiley-Vch, New York*, page 421, 1999.

[16] M. Sahal et al. Structural,electrical and optical properties of ZnO thin films deposited bys olgel method. *Microelectronics Journal*, l39:14251428, 2008.

[17] Ziaul Raza Khan et al. Optical and structural properties of ZnO thin films fabricated by sol-gel method. *Materials Sciences and Applications*, 2:340–345, 2011.

[18] P.S. Gupta Nanda Shakti. Structural and optical properties of sol-gel prepared ZnO thin film. *Applied Physics Research*, 2(1):340–345, May 2010.

[19] Youssef Ammaih et al. Structural, optical and electrical properties of ZnO:Al thin films for optoelectronic applications. *Opt Quant Electron*, 46:229234, 2014.

[20] M. CAGLAR S. ILICAN, Y. CAGLAR. Preparation and characterization of ZnO thin films deposited by sol-gel spin coating method. *Journal of Optoelectronics and Advanced Materials*, 10(10):2578 – 2583, October 2008.

[21] K. Gopalakrishna Naik Shashidhara Bhat, Shrisha B. V. Properties of al doped ZnO thin films grown by spray pyrolysis. *Archives of Physics Research*, 4(4):20–27, 2013.

[22] Nadia Chahmat et al. Effect of sn doping on the properties of ZnO thin films prepared by spray pyrolysis. *Journal of Modern Physics*, 3:1781–1785, 2012.

[23] Erdal Sonmez. Study of structural and optical properties of zinc oxide rods grown on glasses by chemical spray pyrolysis. *Journal of Nanomaterials*, 2012.

[24] S. Kachhwaha Ankit Goyal. ZnO thin films preparation by spray pyrolysis and electrical characterization. *Materials Letters*, 68:354356, 2012.

[25] Annapu Reddy Venkateswarlu et al. Optical and electrical properties of spray pyrolysis deposited nano-crystalline $BiFeO_3$ films. *AIP Advances*, 1, 2011.

[26] D J Huang et al. Optical properties of $BiFeO_3$ and $Bi_{0.9}La_{0.1}FeO_3$ films on silicon substrates. *Journal ofPhysics:ConferenceSeries*, 276, 2011.

[27] C. Himcinschi et al. Substrate influence on the optical and structural properties of pulsed laser deposited $BiFeO_3$ epitaxial films. *Journal of Applied Physics 107*, 107, 2010.

[28] Seo-Hyeon Jo et al. Fabrication and electrical properties of pzt/bfo multilayer thin films. *Transactions on Electrical and Electronic Materials*, 12(5):193–196, October 25 2011.

[29] Z.-H.Wang et al. Multiferroic properties of $BiFeO_3$ ceramic and thin film and $BiFeO_3$/Co/$BiFeO_3$ multi layer structure. *IEEE Transactions on Magnetics*, 45, 2009.

[30] N.F. Mott. *Phil. Mag.*, 19:835, 1969.

[31] P.D. Babu V. Siruguri P.N. Vishwakarma J. Ray, A.K. Biswal. Magnetoelectricity in $BiFeO_3$ and $BiFe_{0.98}Co_{0.02}O_3$ nano particles. *Journal of Alloys and Compounds*, 628:32–38, 2015.

[32] J.K. Wigmore P.V.E. McClintock, D.J. Meredith. Matter at low temperatures blackie. 1984.